Simultaneous Downstream and Upstream Output-Feedback Stabilization of Cascaded Freeway Traffic

Huan Yu, Jean Auriol, Miroslav Krstic

Simultaneous Downstream and Upstream Output-Feedback Stabilization of Cascaded Freeway Traffic

Huan Yu [a,⋆], Jean Auriol [b] and Miroslav Krstic [a]

[a] *Department of Mechanical and Aerospace Engineering, University of California, San Diego, La Jolla, CA, 92093, USA*

[b] *Université Paris-Saclay, CNRS, CentraleSupélec, Laboratoire des Signaux et Systèmes, 91190, Gif-sur-Yvette, France*

Abstract

In this paper, we develop boundary output feedback control laws for the simplest nontrivial example of a traffic flow network system: two cascaded freeway segments connected by a junction. The macroscopic traffic dynamics are governed by the Aw-Rascle-Zhang (ARZ) network model in which two subsystems of second-order nonlinear partial differential equations (PDEs) describe the evolution of traffic density and velocity on each segment. Due to the change of road access at the junction, different equilibria are considered for the two connected segments. To suppress stop-and-go traffic oscillations on the cascaded roads, we consider a ramp metering that regulates the traffic flow rate entering from the on-ramp to the mainline freeway. Different control designs are proposed such that the output feedback stabilization is realized with either the ramp metering located at the middle junction or the outlet with only boundary measurements of flow rate and velocity. The control objective is to simultaneously stabilize the upstream and downstream traffic to a given spatially-uniform constant steady-state. The distinct actuation locations motivate our design of two different delay-robust full state feedback control laws. The proposed designs are based on the PDE backstepping methodology and guarantee the exponential stability of the under-actuated network of two systems of two hyperbolic PDEs. Two types of collocated boundary observers are proposed to construct output feedback controllers where the sensor location is the same as the actuator location. Numerical simulations are performed to validate the control designs. The two collocated output feedback controllers are compared for their stabilization performance. Robustness to delays is also investigated. The proposed controllers are also compared with some Proportional Integral (PI) boundary feedback controllers.

Key words: ARZ traffic network; output feedback; boundary observer: PDE backstepping.

1 Introduction

Freeway traffic modeling and management have been intensively investigated over the past decades. Various models from microscopic to macroscopic have been developed for freeway traffic and numerous control approaches have been applied to mitigate the traffic congestion.

1.1 Macroscopic modeling of traffic network

Macroscopic modeling is well-established to describe freeway traffic dynamics since the aggregated state values used by the models are easy to sense and actuate, leading to a particular interest in freeway traffic management. The macroscopic models predict the evolution of continuous traffic states in the temporal and spatial domain by employing hyperbolic PDEs to govern the dynamics of traffic density and velocity. The most widely-used macroscopic traffic PDE models include the classical first-order Lighthill-Whitham-Richards (LWR) model [27] [29] and the state-of-art second-order Aw-Rascle-Zhang (ARZ) model [2] [33]. The LWR model corresponds to the conservation law of the traffic density. It predicts the formation and propagation of traffic shockwaves on the freeway but fails to describe the stop-and-go oscillatory phenomenon [31], which causes unsafe driving conditions, increased fuel consumption, and delays in travel time. Over decades of studies, the second-order ARZ traffic model is then developed to describe this stop-and-go traffic congestion by allowing a velocity PDE added to the LWR model and thus providing a wider variety of dynamics. A family of flow-density relation is parameterized in the ARZ model by characterizing each vehicle's property as opposed to the averaged static dynamics of the flow-density relation depicted by the LWR model. The ARZ traffic model presents as nonlinear second-order hyperbolic PDEs.

More recently, the macroscopic road networks based on the ARZ family of models have been developed in [18] [22]. Considering the problem of suppressing the stop-and-go congested traffic on cascaded freeway segments, it is, therefore, essential to study the state-of-art second-order macroscopic traffic network models. In this work, we adopt the second-order macroscopic traffic network model in [22] for the two cascaded freeway segments. The model is chosen such that the junction connecting the two roads conserves the mass and drivers' properties, as detailed later in the paper. This property is not smooth across the junction in [18]. The

⋆ Corresponding author.

Email addresses: huy015@ucsd.edu (Huan Yu), jean.auriol@centralesupelec.fr (Jean Auriol), krstic@ucsd.edu (Miroslav Krstic).

solution in [22] is a weak solution (in the sense of the conservative variables of the ARZ model) that guarantees the well-posedness of a closed-loop system for our control design. The considered system of two cascaded freeway segments can then be rewritten as a network of two interconnected hyperbolic PDE systems coupled through their boundaries.

1.2 Traffic boundary control strategies

Traffic control strategies have been developed and successfully implemented for the traffic management infrastructures, namely, ramp metering and varying speed limits (VSL). The flow rate from the on-ramp to mainline freeway is controlled by the ramp metering and velocity at a certain location is actuated by the VSL. Boundary feedback control algorithms are studied for traffic regulation on a freeway segment in [6] [23] [35] [39]. Previous contributions of traffic network control strategies, including [11] [19] [20] [38], focus on controlling the spatially discretized approximation of LWR model, namely cell transmission model and its derivation, but the discretized systems sometimes exhibit discrepancies from the original continuous traffic PDE model. [26] develops an optimal control framework based on Hamilton-Jacobi formulation of the LWR model. [21] consider adjoint-based optimization formulation for the control problem of a LWR-based traffic network by regulating nodes of the network.

Boundary control algorithms have been developed for traffic PDE modeling of a single freeway segment in [6] [23] [35] [39]. These control laws are restricted to control problem of traffic on one freeway segment which necessitates certain road homogeneity. Using the integration of ramp metering and VSLs, [39] firstly considers PI boundary control of a cascaded freeway network, which is modeled by the linearized homogeneous AR model. The static errors of boundary conditions are suppressed since the instabilities do not arise from the transport PDEs. This paper differs in focusing on the oscillations generated by the in-domain traffic that can only be modeled by the inhomogeneous ARZ model. The PDE backstepping method is firstly used for this traffic network problem. More importantly, the cascaded freeway network is underactuated in this work; namely, feedback design is implemented for only one boundary among the four boundary conditions while all boundaries are actuated in [39]. In practice, only one ramp metering is employed with the proposed control designs. This boundary control problem of the traffic network based on the ARZ PDE model has not been studied to the authors' best knowledge.

Boundary control of the network of hyperbolic PDEs has been intensively studied over the past years. Despite many theoretical results in the literature, boundary control of PDE networks remains a challenging research topic. This is because these systems are underactuated. For practical consideration, only the PDEs located at some nodes of the network can be actuated. To tackle this problem, multiple approaches have been proposed: PI boundary controllers for fully actuated networks [5], flatness based design of feedforward control laws for tree-like transmission networks [30]. While the backstepping approach has been successfully applied to design boundary controls for a large class of hyperbolic PDE system [1] [12] [9], the considered system always have (at least) one boundary which is fully actuated. Recently [4] develops backstepping-based state feedback control laws for the underactuated network of hyperbolic PDEs. This class of system is used to model the dynamics of many industrial applications, including water networks in open-channels, communication networks, and gas networks in pipeline. In this paper, we will develop backstepping PDE output feedback controllers for the underactuated traffic network system. To the best of the authors' knowledge, this problem has never been studied before.

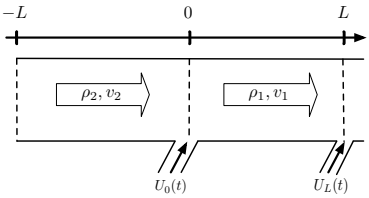

Fig. 1. Traffic flow on upstream and downstream roads of a junction, actuation is implemented at the junction or at the outlet of the downstream road segment.

1.3 New challenges and contribution

In the authors' previous work [35], backstepping boundary control laws for ramp metering are designed to suppress the stop-and-go traffic oscillations on the freeway either upstream or downstream of the ramp. As shown in Fig 1, the traffic flow rate is actuated through on-ramp traffic lights so that either the upstream or the downstream traffic is stabilized. Such control design can not stabilize the two segments simultaneously, and distinct traffic scenarios appearing on the cascaded segments are not addressed by the model. Ramp metering control of the upstream traffic may cause congestion for downstream traffic and vice versa. In the conference versions of our work, we propose a full-state feedback control from the middle boundary [36] and an anti-collocated output feedback controller [37].

This paper's contributions are twofold: First, novel PDE backstepping output feedback controllers and observers are developed for under-actuated hyperbolic PDE system which has not been studied before in theory for such class of system; Second, we provide answers to relevant traffic flow control questions by firstly applying advanced backstepping control for cascaded freeway traffic. This paper introduces output-feedback control designs that simultaneously stabilize the traffic on two cascaded segments modeled as an underactuated fourth-order PDE system. The actuation and measurement are only taken from either the middle junction or the outlet. Four output-feedback controllers are proposed, as shown in Table. 1: two collocated and two anti-collocated ones. They are robust to input delays. This paper also provides a conclusive comparison between the PI and backstepping controllers for the stabilization of the cascaded freeway traffic.

Notation. For any function of two variables $f(x,t)$ defined on $x \in [0,L], t \in [0,\infty)$, the L^2-norm is denoted as

Table 1
Output feedback law

actuator/sensor location	sensor $x=0$	sensor $x=L$
actuator at $x=0$	collocated	anti-collocated
actuator at $x=L$	anti-collocated	collocated

$||f||^2 := \int_0^L f(x,t)^2 dx$. For L^2 function, $f(x,t) \in L^2([0,T])$ denotes $\int_0^T f(x,t)^2 dt < \infty$. and $f(x,t) \in L^2([0,L])$ denotes $\int_0^L f(x,t)^2 dx < \infty$. For any bounded set $\mathscr{T}$ of $\mathbb{R}^2$, we denote $\mathscr{B}(\mathscr{T})$ the set of bounded real functions on $\mathscr{T}$. This set is a Banach space for the sup-norm. We define the following sets: $\mathscr{T}_1 = \{(x,\xi) \in [0,L]^2,\ \xi \geq x\}$, $\bar{\mathscr{T}}_1 = \{(x,\xi) \in [0,L]^2,\ \xi \leq x\}$, $\mathscr{T}_2 = \{(x,\xi) \in [-L,0]^2,\ \xi \leq x\}$, $\bar{\mathscr{T}}_2 = \{(x,\xi) \in [-L,0]^2,\ \xi \geq x\}$, $\mathscr{T} = \{(x,\xi) \in [0,L] \times [-L,0]\}$, and $\bar{\mathscr{T}} = \{(x,\xi) \in [-L,0] \times [0,L]\}$.

2 Problem Statement

We consider a road network that consists of two connected road segments with unidirectional traffic flow and different road conditions, as shown in Fig 1. The two segments are assumed to be the same length for simplicity of notation. The spatial scaling can be easily made for equations that describe traffic states on segments with different lengths.

2.1 ARZ PDE traffic network model

The evolution of traffic density $\rho_1(x,t)$ and velocity $v_1(x,t)$ (with $(x,t) \in [0,L] \times [0,\infty)$) on the downstream road segment and traffic density $\rho_2(x,t)$ and velocity $v_2(x,t)$ ($(x,t) \in [-L,0] \times [0,\infty)$) on the upstream road segment are modeled by the following ARZ model.

$$\partial_t \rho_i + \partial_x(\rho_i v_i) = 0, \tag{1}$$

$$\partial_t(\rho_i(v_i+p_i)) + \partial_x(\rho_i v_i(v_i+p_i)) = -\frac{\rho_i(v_i - V(\rho_i))}{\tau_i}, \tag{2}$$

where PDE states $\rho_i, v_i : [0,L] \times [0,\infty) \to \mathbb{R}^+$ and $i \in \{1,2\}$ represents downstream and upstream road respectively. The labeling of freeway segments is chosen as the reverse direction of traffic flow but same as the propagation direction of the control signal, which will be explained later. The traffic pressure $p_i(\rho_i)$ is defined as an increasing function of the density $p_i(\rho_i) = c_i \rho_i^{\gamma_i}$, where $\gamma_i, c_i \in \mathbb{R}^+$ is defined as $c_i = v_m/\rho_{m,i}^{\gamma_i}$. The coefficient γ_i represents the overall drivers' property, reflecting their change of driving behavior to the increase of density. The positive constant v_m represents the maximum velocity and the positive constant $\rho_{m,i}$ is the maximum density defined as the number of vehicles per unit length. The equilibrium density-velocity relation $V_i(\rho_i)$ is given by $V(\rho_i) = v_m - p_i(\rho_i)$ for both segments, which assumes the same maximum velocity for the two segments when there are no vehicles on the road $\rho_i = 0$. We define the following variable

$$w_i = v_i + p_i(\rho_i), \tag{3}$$

which is interpreted as traffic "friction" or drivers' property [17]. This property transports in the traffic flow with vehicle velocity, representing the heterogeneity of individual driver with respect to the equilibrium density-velocity relation $V_i(\rho_i)$. The maximum velocity v_m is assumed to be the same for the two road segments while the maximum density $\rho_{m,i}$ and coefficient γ_i are allowed to vary. The positive constant τ_i is the relaxation time that represents the time scale for traffic velocity v_i adapting to the equilibrium density-velocity relation $V_i(\rho_i)$. We denote the traffic flow rate on each road as $q_i = \rho_i v_i$. The equilibrium flow and density relation, also known as the fundamental diagram, is then given by $Q_i(\rho_i) = \rho_i V(\rho_i) = \rho_i v_m \left(1 - (\rho_i/\rho_{m,i})^{\gamma_i}\right)$.

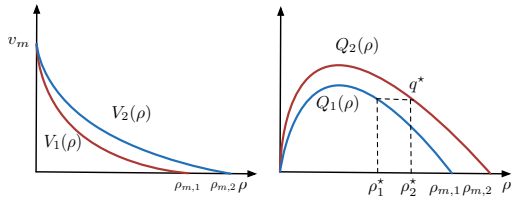

Fig. 2. The equilibrium density and velocity relation $V_i(\rho)$ on the left, the equilibrium density and flux relation $Q_i(\rho)$ on the right

We consider the situation that the upstream road segment 2 for $x \in [-L,0]$ has more lanes than the downstream road segment for $x \in [0,L]$, in which congested traffic is usually formed up from downstream to upstream. Therefore, the maximum density $\rho_{m,2} > \rho_{m,1}$. The maximum driving speed v_m is assumed to be the same for the two segments. The critical density ρ_c segregates the free and congested regimes of traffic states. The critical density is given by $\rho_{c,i} = \rho_{m,i}/(1+\gamma_i)^{1/\gamma_i}$ such that $Q_i'(\rho)|_{\rho=\rho_c} = 0$. The traffic is free when the density satisfies $\rho < \rho_{c,i}$. The traffic is defined as the congested one when the density satisfies $\rho > \rho_{c,i}$. The traffic is defined as the congested one when the density satisfies $\rho > \rho_{c,i}$. For the free traffic, oscillations around the steady states will be damped out fast. For the congested traffic, there are two directional waves on road with one being the velocity oscillation propagating upstream and the other one being the density oscillation propagating downstream with the traffic.

2.2 Actuated boundary from two different locations

Regarding the boundary conditions connecting the two PDE systems, the Rankine-Hugoniot condition is satisfied at the junction such that the weak solution exists for the network (1)-(2). This condition implies piecewise smooth solutions and corresponds to the conservation of the mass and of the drivers' properties defined in (3) at the junction. Thus the flux and drivers' property are assumed to be continuous across the boundary conditions at $x = 0$, that is

$$\rho_1(0,t)v_1(0,t) = \rho_2(0,t)v_2(0,t), \tag{4}$$

$$w_2(0,t) = w_1(0,t). \tag{5}$$

For open-loop system, we assume a constant inflow $q^\star$ entering the inlet boundary $x = -L$ and a constant outflow $q^\star$ at the outlet boundary for $x = L$:

$$q_2(-L,t) = q^\star, \tag{6}$$

$$q_1(L,t) = q^\star, \tag{7}$$

The control problem we solve consists in stabilizing the traffic flow in both the upstream and downstream road segments

with a single actuator. Three possible locations for implementing a ramp metering control input are either at the inlet $x=-L$, at the junction $x=0$ or at the outlet $x=L$. We only present the control and estimation results for control input either from the middle junction or from the outlet, as shown in Fig.1. Actuation at the inlet is a less challenging control problem that can be solved following [35] by reducing the traffic inflow. Except for the controlled boundaries, the boundary conditions remain to be the same with the open-loop system in (4)-(7).

Ramp metering control $U_0(t)$ from the junction $x=0$: The traffic flow entering from the junction to the mainline road is controlled by $U_0(t)$. Given the flux continuity condition, the boundary condition at the junction is

$$q_1(0,t) = q_2(0,t) + U_0(t), \tag{8}$$

where the downstream segment flow consists of the inflow from the mainline upstream segment and the actuated traffic flow from the on-ramp.

Ramp metering control $U_L(t)$ from the outlet $x=L$: The downstream outflow at $x=L$ is actuated by $U_L(t)$,

$$q_1(L,t) = q^\star + U_L(t), \tag{9}$$

where the outflow rate equals to the summation of the on-ramp metering flow and the constant mainline flow. In what follows, when we implement one choice of control input, the other control input equals to zero. It should be noted that the designed controllers U_0 in (35) and U_L in (49) are the flow rate perturbations around a nominal flow rate.

2.3 Linearized model in the Riemann coordinates

We are concerned with the congested traffic and assume that the equilibrium of both segments $(\rho_1^\star, v_1^\star)$, $(\rho_2^\star, v_2^\star)$ are in the congested regime, which is the only one of theoretical control interest among all four traffic scenarios including free and free, free and congested, congested and free, congested and congested. The steady states $(\rho_1^\star, v_1^\star)$, $(\rho_2^\star, v_2^\star)$ are considered to be in the congested regime and the boundary conditions (4) and (5) are satisfied, i.e.,

$$\rho_1^\star v_1^\star = \rho_2^\star v_2^\star = q^\star, \tag{10}$$

$$w_1^\star = w_2^\star = v_m, \tag{11}$$

where the steady state velocities satisfy the equilibrium density-velocity relation $v_i^\star = V_i(\rho_i^\star)$. According to (3), the constant driver's property in (11) implies that we have the same maximum velocity v_m for the two segments (which corresponds to our initial assumption): $v_1^\star + p_1^\star = v_2^\star + p_2^\star = v_m$, where $p_i^\star = p_i(\rho_i^\star)$.

We linearize the ARZ based traffic network model (ρ_i, v_i) in (1), (2) with the boundary conditions (4), (5), (6), (7) around the steady states $(\rho_i^\star, v_i^\star)$. In order to obtain simplify the model for control design, the linearized model is then rewritten into the Riemann variables and then a invertible spatial transformation is applied

$$\tilde{w}_i = \exp\left(\frac{x}{\tau_i v_i^\star}\right)\left(\frac{\gamma_i p_i^\star}{q^\star}(\rho_i v_i - \rho_i^\star v_i^\star) + \frac{1}{r_i}(v_i - v_i^\star)\right), \tag{12}$$

$$\tilde{v}_i = v_i - v_i^\star, \tag{13}$$

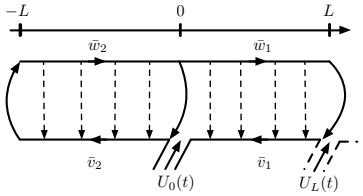

Fig. 3. Control diagram for the closed-loop system with either the actuation from the middle junction $x=0$ or from the outlet $x=L$.

where the constant coefficients r_i are defined as $r_i = -\frac{v_i^\star}{\gamma_i p_i^\star - v_i^\star}$. For the congested regime we have $\rho_i^\star > \frac{\rho_{m,i}}{(1+\gamma_i)^{1/\gamma_i}}$ so that the characteristic speed $\gamma_i p_i^\star - v_i^\star > 0$. The velocity variations $\tilde{v}_i(x,t)$ transport upstream which means the action of velocity acceleration or deceleration is repeated from the leading vehicle to the following vehicle.

With such a change of variable, the linearized system with the controlled boundary conditions (8) and (9) rewrites as

$$\partial_t \tilde{w}_i + v_i^\star \partial_x \tilde{w}_i = 0, \tag{14}$$

$$\partial_t \tilde{v}_i - (\gamma_i p_i^\star - v_i^\star)\partial_x \tilde{v}_i = c_i(x)\tilde{w}_i, \tag{15}$$

$$\tilde{w}_1(0,t) = \tilde{w}_2(0,t), \tag{16}$$

$$\tilde{v}_1(L,t) = r_1 \exp\left(\frac{-L}{\tau_1 v_1^\star}\right)\tilde{w}_1(L,t) + \frac{1-r_1}{\rho_1^\star}U_L(t), \tag{17}$$

$$\tilde{w}_2(-L,t) = \exp\left(\frac{-L}{\tau_2 v_2^\star}\right)\frac{1}{r_2}\tilde{v}_2(-L,t), \tag{18}$$

$$\tilde{v}_2(0,t) = \delta\frac{r_2}{r_1}\tilde{v}_1(0,t) + r_2(1-\delta)\tilde{w}_2(0,t) + \frac{1-r_2}{\rho_2^\star}U_0(t), \tag{19}$$

where the spatially varying coefficients $c_i(x)$ are defined as $c_i(x) = -\frac{1}{\tau_i}\exp\left(-\frac{x}{\tau_i v_i^\star}\right)$. and the constant coefficient δ is $\delta = \frac{\gamma_2 p_2^\star}{\gamma_1 p_1^\star} > 0$. The constant δ represents the ratio related to the traffic pressure of the segments. Derivation of the linearization and the spatial transformation is straightforward to obtain by following [35] and thus are omitted here. The control diagram is shown in Fig. 3 for the transformed system (14)-(19). The well-posedness (in the weak sense) of the linearized system (14)-(19) is stated in [6, Theorem A.4]. The control operator is admissible: in presence of L^2 control inputs and for any initial conditions $(\tilde{v}_0)_1, (\tilde{w}_0)_1 \in (L^2([0,L]))^2$ and $(\tilde{v}_0)_2, (\tilde{w}_0)_2 \in (L^2([-L,0]))^2$, there is only one L^2-solution. It is shown in [35] that only marginal linear stability holds for the open-loop system of one segment. Our objective is to design the control law $U_0(t)$ or $U_L(t)$ to stabilize the system (14)-(19) in the sense of the L^2-norm. Note that we could obtain more regular solutions (strong solutions) by imposing some additional regularity conditions on the initial conditions or the coupling terms, and adding compatibility conditions (see [6] for instance). We make the following non-restrictive assumption so that the proposed feedback laws have some (delay)-robustness margins.

Assumption 1 *The boundary couplings of the system* (14)-(19) *are such that*

$$\delta < \frac{1+\exp(\frac{L}{\tau_2 v_2^\star})}{1+\exp(\frac{-L}{\tau_1 v_1^\star})}. \tag{20}$$

If this assumption is not satisfied, then it is not possible to robustly stabilize the system (14)-(19) when there are input delays (as the open-loop transfer function would have an infinite chain of poles in the complex right half-plane).

3 State feedback Control Designs

In this section, we design full-state feedback laws that guarantee the stabilization of the system (14)-(19) for the different actuation locations. In each case, the backstepping method is employed. Using a Volterra transformation (eventually combined with an affine transformation in the case of the actuation located at the outlet), we map the original under-actuated system to a target system for which the in-domain coupling terms c_1 and c_2 have been moved at the actuated boundary in the form of integral couplings. We can then use the actuation to eliminate these terms. The resulting system is exponentially stable due to Assumption 1. As such a control law does not modify the boundary couplings, it is strictly proper, and consequently, the robustness margins are preserved (see [3] for details).

3.1 Feedback law $U_0(t)$ with flow rate control from $x=0$

The control input $U_0(t)$ for full-state feedback stabilization is given by

$$U_0(t) = \frac{\rho_2^\star}{1-r_2}\left(\int_{-L}^{0} K_2^{vw}(0,\xi)\tilde{w}_2(\xi,t) + K_2^{vv}(0,\xi)\tilde{v}_2(\xi,t)d\xi \right.$$
$$\left. - \delta\frac{r_2}{r_1}\int_0^L K_1^{vw}(0,\xi)\tilde{w}_1(\xi,t) + K_1^{vv}(0,\xi)\tilde{v}_1(\xi,t)d\xi\right) \tag{21}$$

More details of the control design can be found in [36]. This control input is a L^2 function. For any initial conditions $(\tilde{v}_0)_1, (\tilde{w}_0)_1 \in (L^2([-L,0]))^2$ and $((\tilde{v}_0)_2, (\tilde{w}_0)_2) \in (L^2([-L,0]))^2$, there is only one L^2-solution to the closed-loop system for (14)-(19) with (21). Moreover, since the kernels are bounded functions, our control operator is a linear bounded operator. Consequently, it is a continuous operator. Thus the control law $U_0 : [0,T] \to \mathbb{R}$ is continuous. More regularity can be obtained, if necessary, by increasing the regularity of the coupling coefficients c_i. For practical implementation of the ramp metering control input, we need to modulate the changing frequency of the on-ramp traffic light. The event-triggered control in [16] provides a way to implement the continuous-time controllers into digital forms by updating the input values only when needed. It is strictly proper as it is only composed of integral terms. Following the ideas of [4], we can prove that it is robust with respect to delays in the actuation and uncertainties on the parameters. We have the following theorem.

Theorem 1 *Consider the PDE system* (14)-(19) *with the feedback law U_0 defined in* (21)*. Then, for any L^2 initial condition $(\tilde{w}_i(\cdot,0), \tilde{v}_i(\cdot,0))$, the closed-loop system is exponentially stable at the origin.*

The definition of exponential convergence can be found, e.g., in [6, Definition 3.1].

3.2 Feedback law $U_L(t)$ with flow rate control from $x=L$

We now consider that the available actuation is located at the outlet $x=L$. Our approach is adjusted from [4]. However, the control law given in [4] is obtained after two successive backstepping transformations since it makes the well-posedness proof of kernels easier. We choose here to do it using only one transformation, as we already know that such a transformation exists.

$$\bar{\alpha}_1(x,t) = \tilde{w}_1(x,t), \tag{22}$$
$$\bar{\beta}_1(x,t) = \tilde{v}_1(x,t) - \int_0^x \bar{K}_1^{vw}(x,\xi)\tilde{w}_1(\xi,t)d\xi$$
$$- \int_0^x \bar{K}_1^{vv}(x,\xi)\tilde{v}_1(\xi,t)d\xi - \int_{-L}^0 M^w(x,\xi)\tilde{w}_2(\xi,t)d\xi$$
$$- \int_{-L}^0 M^v(x,\xi)\tilde{v}_2(\xi,t)d\xi, \tag{23}$$
$$\bar{\alpha}_2(x,t) = \tilde{w}_2(x,t), \tag{24}$$
$$\bar{\beta}_2(x,t) = \tilde{v}_2(x,t) - \int_{-L}^x \bar{K}_2^{vw}(x,\xi)\tilde{w}_2(\xi,t)d\xi$$
$$- \int_{-L}^x \bar{K}_2^{vv}(x,\xi)\tilde{v}_2(\xi,t)d\xi, \tag{25}$$

where the kernels $\bar{K}_1^{vw}$ and $\bar{K}_1^{vv}$ are defined on the set $\bar{\mathscr{T}}_1$, the kernels $\bar{K}_2^{vw}$ and $\bar{K}_2^{vv}$ are defined on the set $\mathscr{T}_2$. Finally the kernels M^w and M^v are bounded functions defined on $\mathscr{T}$. Note that the transformation (24)-(25) is invertible (as it is a Volterra transformation [34, Chapter 4]). Thus, the first transformation (22)-(23) is invertible as it is a combination of a Volterra transformation with an affine transformation. The different kernels satisfy the following set of PDEs on their corresponding domains of definition

$$(\gamma_i p_i^\star - v_i^\star)\partial_x \bar{K}_i^{vw} - v_i^\star \partial_\xi \bar{K}_i^{vw} = c_i(\xi)\bar{K}_i^{vv}, \tag{26}$$
$$\partial_x \bar{K}_i^{vv} + \partial_\xi \bar{K}_i^{vv} = 0, \tag{27}$$
$$(\gamma_1 p_1^\star - v_1^\star)\partial_x M^v + (\gamma_2 p_2^\star - v_2^\star)\partial_\xi M^v = 0, \tag{28}$$
$$(\gamma_1 p_1^\star - v_1^\star)\partial_x M^w - v_2^\star \partial_\xi M^w = c_2(\xi)M^v, \tag{29}$$

along with the boundary conditions

$$\bar{K}_i^{vw}(x,x) = -\frac{c_i(x)}{\gamma_i p_i^\star}, \ \bar{K}_1^{vv}(x,0) = \frac{v_2^\star}{v_1^\star}\delta M^v(x,0), \tag{30}$$
$$\bar{K}_2^{vv}(x,-L) = -\exp\left(\frac{-L}{\tau_2 v_2^\star}\right)\bar{K}_2^{vw}(x,-L), \tag{31}$$
$$M^w(0,\xi) = \frac{r_1}{\delta r_2}\bar{K}_2^{vw}(0,\xi), \ M^v(0,\xi) = \frac{r_1}{\delta r_2}\bar{K}_2^{vv}(0,\xi), \tag{32}$$
$$M^w(x,0) = (1-\delta)M^v(x,0) + \frac{v_1^\star}{v_2^\star}\bar{K}_1^{vw}(x,0), \tag{33}$$
$$M^v(x,-L) = -\exp\left(\frac{-L}{\tau_2 v_2^\star}\right)M^w(x,-L). \tag{34}$$

We have the following lemma.

Lemma 2 *For system* (26)-(34)*, there exists a unique solution* $\bar{K}_1^{vw}$*,* $\bar{K}_1^{vv}$ *in* $\mathscr{B}(\bar{\mathscr{T}}_1)$*,* $\bar{K}_2^{vw}$*,* $\bar{K}_2^{vv}$ *in* $\mathscr{B}(\mathscr{T}_2)$ *and* M^v, M^w *in* $\mathscr{B}(\mathscr{T})$*.*

PROOF. We start by assessing the existence of $\bar{K}_2^{vw}$ and $\bar{K}_2^{vv}$ using [9]. The rest of the proof is based on an induction argument and is adjusted from the one given in [4, Lemma 2]. Let us define $\chi = \frac{\gamma_2 p_2^\star - v_2^\star}{v_2^\star}$ and let us define the sequence x_k by

$$x_k = \min(\chi \times k, 1).$$

Let us now define the following triangular domains defined for $k \geq 1$.

$$\mathscr{R}_k = \{(x,\xi) \in [0,1]\times[-1,0],\ \xi \leq -\frac{1}{\chi}(x - x_{k-1})\},$$
$$\bar{\mathscr{R}}_k = \{(x,\xi) \in [0,1]\times[-1,0],\ \xi \geq -\frac{1}{\chi}(x - x_{k-1})\},$$
$$\mathscr{S}_k = \{(x,\xi) \in [0,x_k]^2,\ x \geq \xi\}$$

Applying [15, Theorem 3.2] on equation (28)-(29) with the boundary conditions (32) and (34), we can prove the existence of the kernels M^v and M^w on the triangular domain $\mathscr{R}_1$. Consequently, these kernels are defined on the line $x = -\chi\xi$. Let us now perform the change of variables $\bar{\xi} = -\frac{1}{\chi}\xi$ to map the domain $\mathscr{S}_1$ to $\bar{\mathscr{R}}_1$. Consequently, we can express the kernels $\bar{K}_1^{\cdot\cdot}$ on the domain $\bar{\mathscr{R}}_1$ (when $x \leq \chi$). We denote by $\hat{K}_1$ the corresponding kernels after this change of variables. Again, we can apply [15, Theorem 3.2] to prove the existence of the kernels M^w, M^v and $\hat{K}_1^{\cdot\cdot}$ on $\bar{\mathscr{R}}_1$. This imply the existence of $\bar{K}_1^{\cdot\cdot}$ on $\mathscr{S}_1$. We then iterate the procedure on the intervals $[x_{k-1}, x_k]$ to conclude the proof. □

The kernels here are bounded functions (instead of continuous functions) since we decided to apply the results from [15, Theorem 3.2]. This theorem has been stated in a more general framework where the kernels may present some discontinuities. However, these discontinuities occur along the characteristic lines and do not have any consequence on the backstepping transformation. Adjusting the proof given in [15], it is possible to show that the kernels are piecewise continuous functions whose discontinuities occur along the characteristic lines. Again, more regularity can be obtained, if necessary, by increasing the regularity of the coupling coefficients c_i. The transformation (23)-(25) maps the original system (14)-(19) to the following decoupled target system

$$\partial_t \alpha_i + v_i^\star \partial_x \alpha_i = 0, \tag{35}$$
$$\partial_t \beta_i - (\gamma_i p_i^\star - v_i^\star)\partial_x \beta_i = 0, \tag{36}$$
$$\alpha_1(0,t) = \alpha_2(0,t), \tag{37}$$
$$\beta_1(L,t) = r_1 \exp\left(-\frac{L}{\tau_1 v_1^\star}\right)\alpha_1(L,t), \tag{38}$$
$$\alpha_2(-L,t) = \exp\left(\frac{-L}{\tau_2 v_2^\star}\right)\frac{1}{r_2}\beta_2(-L,t), \tag{39}$$
$$\beta_2(0,t) = \delta\frac{r_2}{r_1}\beta_1(0,t) + r_2(1-\delta)\alpha_2(0,t). \tag{40}$$

The control input $U_L(t)$ is obtained as

$$U_L(t) = \frac{\rho_1^\star}{1-r_1}\left(\int_0^L \bar{K}_1^{vw}(L,\xi)w_1(\xi,t)d\xi + \bar{K}_1^{vv}(L,\xi)v_1(\xi,t)d\xi + \int_{-L}^0 M^w(L,\xi)w_2(\xi,t)d\xi + M^v(L,\xi)v_2(\xi,t)d\xi\right). \tag{41}$$

We have the following theorem.

Theorem 3 *Consider the PDE system* (14)-(19) *with the feedback law* U_L *defined in* (41)*. Then, for any* L^2 *initial condition* $(\tilde{w}_i(\cdot,0), \tilde{v}_i(\cdot,0))$*, the closed-loop system is exponentially stable at the origin.*

4 Boundary Observer Designs

The control laws designed in the previous section require the value of the state all over the spatial domain. Therefore we design boundary observers which either rely on the measurement of traffic states from the junction or from the outlet of the system.

4.1 Observer with measurement $Y_0(t)$ *at* $x = 0$

This section discusses the case of an observer that relies on the measurement of $\tilde{q}_i$ and $\tilde{v}_i$ at the left side of the junction. Since it holds that $\tilde{w}_2(0,t) = \frac{\gamma_2 p_2^\star}{q^\star}\tilde{q}_2(0,t) - \frac{1}{r_2}\tilde{v}_2(0,t)$, we consider that the following measurement is available

$$Y_0(t) = \tilde{w}_2(0,t). \tag{42}$$

The observer equation are proposed in [37]. They are a copy of the original dynamics with output injection gains. They read as follows

$$\partial_t \hat{w}_i + v_i^\star \partial_x \hat{w}_i = -\phi_i(x)(\tilde{w}_2(0,t) - \hat{w}_i(0,t)), \tag{43}$$
$$\partial_t \hat{v}_i - (\gamma_i p_i^\star - v_i^\star)\partial_x \hat{v}_i = c_i(x)\hat{w}_i - \chi_i(x)(\tilde{w}_2(0,t) - \hat{w}_i(0,t)), \tag{44}$$
$$\hat{w}_1(0,t) = \hat{w}_2(0,t), \tag{45}$$
$$\hat{v}_1(L,t) = r_1 \exp\left(\frac{-L}{\tau_1 v_1^\star}\right)\hat{w}_1(L,t) + \frac{1-r_1}{\rho_1^\star}U_L(t), \tag{46}$$
$$\hat{w}_2(-L,t) = \exp\left(\frac{-L}{\tau_2 v_2^\star}\right)\frac{1}{r_2}\hat{v}_2(-L,t), \tag{47}$$
$$\hat{v}_2(0,t) = \delta\frac{r_2}{r_1}\hat{v}_1(0,t) + (1-\delta)r_2\hat{w}_2(0,t) + \frac{1-r_2}{\rho_2^\star}U_0(t), \tag{48}$$

where $\hat{w}_i(x,t), \hat{v}_i(x,t)$ are the estimates of the state variables $\tilde{w}_i(x,t)$ and $\tilde{v}_i(x,t)$. The terms ϕ_i and χ_i are output injection gains, defined as

$$\phi_1(x) = -v_1^\star N_1^{ww}(x,0), \quad \chi_1(x) = -v_1^\star N_1^{vw}(x,0), \tag{49}$$
$$\phi_2(x) = v_2^\star N_2^{ww}(x,0), \quad \chi_2(x) = v_2^\star N_2^{vw}(x,0), \tag{50}$$

where the kernels N are given in [37].

Theorem 4 *Consider the PDE system* (43)-(48) *with the output injections gains defined in* (49)-(50)*. Then, for any* L^2 *initial condition* $(\hat{w}_i(\cdot,0), \hat{v}_i(\cdot,0))$*, the states* $(\hat{w}_i, \hat{v}_i)$ *exponentially converge to the states* $(\tilde{w}_i, \tilde{v}_i)$*.*

Although the use of the trace operator in (43)-(50) induces a loss of regularity, it is not a problem since the kernels that define the observer gains are regular enough (H^1 functions). Strong solutions remain possible by adding compatibility and regularity conditions.

4.2 Observer with measurement $Y_L(t)$ at $x = L$

In this section, we now assume that the measurement available correspond to the values of $\tilde{q}_i$ and $\tilde{v}_i$ at the left side of the outlet $x = L$. Since we have $\bar{w}_1(L,t) = \exp\left(\frac{L}{\tau_1 v_1^\star}\right)\left(\frac{\gamma_1 p_1^\star}{q^\star}\tilde{q}_1(L,t) - \frac{1}{r_1}\tilde{v}_1(L,t)\right)$, we can consider that the boundary measurement corresponds to

$$Y_L(t) = \tilde{w}_1(L,t). \tag{51}$$

The observer system is given by

$$\partial_t \hat{w}_i + v_i^\star \partial_x \hat{w}_i = -\mu_i(x)(\tilde{w}_1(L,t) - \hat{w}_1(L,t)), \tag{52}$$

$$\partial_t \hat{v}_i - (\gamma_i p_i^\star - v_i^\star)\partial_x \hat{v}_i = c_i(x)\hat{w}_i - \nu_i(x)(\tilde{w}_1(L,t) - \hat{w}_1(L,t)), \tag{53}$$

$$\hat{w}_1(0,t) = \hat{w}_2(0,t), \tag{54}$$

$$\hat{v}_1(L,t) = r_1 \exp\left(-\frac{L}{\tau_1 v_1^\star}\right)\hat{w}_1(L,t) + \frac{1-r_1}{\rho_1^\star}U_L(t), \tag{55}$$

$$\hat{w}_2(-L,t) = \exp\left(\frac{-L}{\tau_2 v_2^\star}\right)\frac{1}{r_2}\hat{v}_2(-L,t), \tag{56}$$

$$\hat{v}_2(0,t) = \delta\frac{r_2}{r_1}\hat{v}_1(0,t) + (1-\delta)r_2\hat{w}_2(0,t) + \frac{1-r_2}{\rho_2^\star}U_0(t), \tag{57}$$

where $\hat{w}_i(x,t), \hat{v}_i(x,t)$ are the estimates of the state variables $\tilde{w}_i(x,t)$ and $\tilde{v}_i(x,t)$. The terms μ_i and ν_i are output injection gains that still have to be designed. They are bounded functions (actually piecewise continuous) respectively defined on $([0,L])^2$ and $([-L,0])^2$. The corresponding initial conditions of the observer are L^2 functions. Defining the error estimates $\check{w}_i = \tilde{w}_i - \hat{w}_i$ and $\check{v}_i = \tilde{v}_i - \hat{v}_i$, the error system is obtained by subtracting the observer equations in (53)-(57) from (14)-(19). Let us consider the following backstepping transformations

$$\check{\alpha}_1(x,t) = \check{w}_1(x,t) - \int_x^L \bar{N}_1^{ww}(x,\xi)\check{w}_1(\xi,t), \tag{58}$$

$$\check{\beta}_1(x,t) = \check{v}_1(x,t) - \int_x^L \bar{N}_1^{vw}(x,\xi)\check{w}_1(\xi,t)d\xi, \tag{59}$$

$$\check{\alpha}_2(x,t) = \check{w}_2(x,t) - \int_x^0 \bar{N}_2^{ww}(x,\xi)\check{w}_2(\xi,t)d\xi - \int_0^L F^w(x,\xi)\check{w}_1(\xi,t)d\xi, \tag{60}$$

$$\check{\beta}_2(x,t) = \check{v}_2(x,t) - \int_x^0 \bar{N}_2^{vw}(x,\xi)\check{w}_2(\xi,t)d\xi - \int_0^L F^v(x,\xi)\check{w}_1(\xi,t)d\xi, \tag{61}$$

where the kernels $\bar{N}_1^{ww}$ and $\bar{N}_1^{wv}$ are bounded functions defined on the set $\mathscr{T}_1$, while the kernels $\bar{N}_2^{ww}$ and $\bar{N}_2^{wv}$ are bounded functions defined on the set $\bar{\mathscr{T}}_2$. The kernels F^α and F^β are bounded functions defined on the set $\bar{\mathscr{T}}$. Note that the transformation (58)-(59) is invertible (as it is a Volterra transformation [34]). The transformation (60)-(61) is a combination of a Volterra transformation with an affine transformation and is consequently invertible. The kernels satisfy the following set of PDEs:

$$(\gamma_i p_i^\star - v_i^\star)\partial_x \bar{N}_i^{vw}(x,\xi) - v_i^\star \partial_\xi \bar{N}_i^{vw}(x,\xi) = 0, \tag{62}$$

$$\partial_x \bar{N}_i^{ww}(x,\xi) + \partial_\xi \bar{N}_i^{ww}(x,\xi) = 0, \tag{63}$$

$$v_2^\star \partial_x F^w(x,\xi) + v_1^\star \partial_\xi F^w(x,\xi) = 0, \tag{64}$$

$$(\gamma_2 p_2^\star - v_2^\star)\partial_x F^v(x,\xi) - v_1^\star \partial_\xi F^v(x,\xi) = 0, \tag{65}$$

with the boundary conditions

$$\bar{N}_2^{vw}(x,x) = \frac{c_2(x)}{\gamma_2 p_2^\star},\ \bar{N}_1^{vw}(x,x) = \frac{c_1(x)}{\gamma_1 p_1^\star}, \tag{66}$$

$$\bar{N}_2^{ww}(-L,\xi) = \exp(-\frac{L}{\tau_2 v_2^\star})\frac{1}{r_2}\bar{N}_2^{vw}(-L,\xi) \tag{67}$$

$$F^v(x,0) = \frac{v_2^\star}{v_1^\star}\bar{N}_2^{vw}(x,0),\ F^w(x,0) = \frac{v_2^\star}{v_1^\star}\bar{N}_2^{ww}(x,0), \tag{68}$$

$$F^w(-L,\xi) = \exp(\frac{-L}{\tau_2 v_2^\star})\frac{1}{r_2}F^v(-L,\xi), \tag{69}$$

$$F^v(0,\xi) = \delta\frac{r_2}{r_1}\bar{N}_1^{vw}(0,\xi) + (1-\delta)r_2 F^w(0,\xi), \tag{70}$$

$$\bar{N}_1^{ww}(0,\xi) = F^w(0,\xi), \tag{71}$$

The well-posedness of this kernel PDE-system is guaranteed by the following lemma.

Lemma 5 *Consider system* (62)-(71). *There exists a unique solution* $\bar{N}_1^{ww}$, $\bar{N}_1^{vw}$ *in* $\mathscr{B}(\mathscr{T}_1)$, $\bar{N}_2^{ww}$, $\bar{N}_2^{vw}$ *in* $\mathscr{B}(\bar{\mathscr{T}}_2)$ *and* F^w, F^v *in* $\mathscr{B}(\bar{\mathscr{T}})$.

PROOF. The well-posedness of the kernels $\bar{N}_2^{ww}$ and $\bar{N}_2^{vw}$ is proved following [32]. Then we prove the well-posedness of the kernels F^w, F^v, $\bar{N}_1^{ww}$ and $\bar{N}_1^{vw}$ adjusting [4, Lemma 2]. □

Let us now define the output injection gains μ_i and ν_i as

$$\mu_1(x) = -v_1^\star \bar{N}_1^{ww}(x,L) + \int_x^L \mu_1(\xi)\bar{N}_1^{ww}(x,\xi)d\xi, \tag{72}$$

$$\nu_1(x) = -v_1^\star \bar{N}_1^{vw}(x,L) + \int_x^L \mu_1(\xi)\bar{N}_1^{vw}(x,\xi)d\xi, \tag{73}$$

$$\mu_2(x) = -v_1^\star F^w(x,L) + \int_x^0 \mu_2(\xi)\bar{N}_2^{ww}(x,\xi)d\xi + \int_0^L \mu_1(\xi)\bar{F}^w(x,\xi)d\xi, \tag{74}$$

$$\nu_2(x) = -v_1^\star F^v(x,L) + \int_x^0 \mu_2(\xi)\bar{N}_2^{vw}(x,\xi)d\xi + \int_0^L \mu_1(\xi)\bar{F}^v(x,\xi)d\xi. \tag{75}$$

These output injection gains are perfectly defined: since (72) is a Volterra equation of second kind, it is invertible and we can obtain μ_1. Once μ_1 is obtained, then equation (74) becomes a Volterra equation and we can compute μ_2. Once μ_1 and μ_2 are obtained, the expressions of ν_1 and ν_2 are explicit. With this choice of injection gains, differentiating the transformations (58)-(59) and (60)-(61) with respect to

time and space, it is straightforward to obtain that the convergence of the observer in the following theorem.

Theorem 6 *Consider the PDE system* (53)-(57) *with the output injections gains defined in* (72)-(73)*. Then, for any L^2 initial condition $(\hat{w}_i(\cdot,0),\hat{v}_i(\cdot,0))$, the states $(\hat{w}_i,\hat{v}_i)$ exponentially converge to the states $(\tilde{w}_i,\tilde{v}_i)$.*

5 Output Feedback Laws

The two state feedback laws and the two observers that we have previously designed are employed to construct four possible output feedback laws, which consist of two collocated and two anti-collocated ones, as shown in Table. 1. We are now able to give the main theorem of this paper.

Theorem 7 *Consider the system* (14)-(19) *with the control law at $x=0$ or at $x=L$*

$$U_0(t)=\frac{\rho_2^\star}{1-r_2}\left(\int_{-L}^{0}K_2^{vw}(0,\xi)\hat{w}_2(\xi,t)+K_2^{vv}(0,\xi)\hat{v}_2(\xi,t)d\xi - \frac{r_2}{r_1}\int_0^L K_1^{vw}(0,\xi)\hat{w}_1(\xi,t)+K_1^{vv}(0,\xi)\hat{v}_1(\xi,t)d\xi\right), \tag{76}$$

$$U_L(t)=\frac{\rho_1^\star}{1-r_1}\left(\int_0^{L}\bar{K}_1^{vw}(L,\xi)\hat{w}_1(\xi,t)d\xi+\bar{K}_1^{vv}(L,\xi)\hat{v}_1(\xi,t)d\xi + \int_{-L}^{0}M^{w}(L,\xi)\hat{w}_2(\xi,t)d\xi+M^{v}(L,\xi)\hat{v}_2(\xi,t)d\xi\right). \tag{77}$$

where the estimated states are either given by equations (43)-(48) *or* (53)-(57)*, depending on the available measurements. Then, for any L^2 initial condition, the closed-loop system with the controller* (76) *or* (77) *is exponentially stable at the origin. This implies the local convergence of the initial states of ρ_i and v_i to the steady states $\rho_i^\star$ and $v_i^\star$.*

6 Simulation results

In this section, we first validate the control design with numerical simulations and compare the two collocated output feedback laws. Then we demonstrate the robustness of the proposed controllers to delays in the actuation path. In the end, our control design is compared with PI boundary controllers, which fully actuate the interconnected system. As stated in Table.1, there are four proposed output feedback controllers, but only the simulation results of the two collocated ones are conducted. The collocated controllers are the most relevant in practice since the anti-collocated sensor and actuator in the distance will have delays and errors caused by long-distance communication.

The length of each freeway segment is chosen to be $L=0.5$ km so the total length of the two connected segments

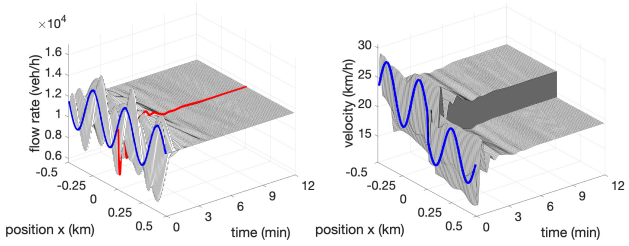

Fig. 4. The closed-loop simulation of traffic flow rate and velocity, with the ramp metering control input $U_0(t)$ and measurement $Y_0(t)$ from the middle junction $x=0$, converges to steady states. The controlled flow rate evolution at $x=0$ is highlighted in red.

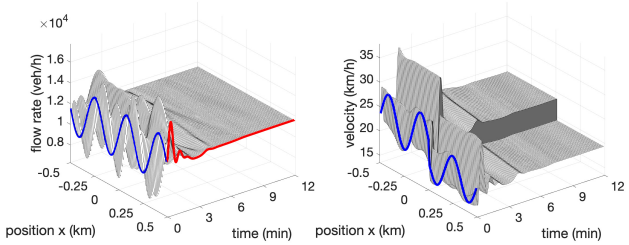

Fig. 5. The closed-loop simulation of traffic flow rate and velocity, with the ramp metering control input $U_L(t)$ and measurement $Y_L(t)$ from the outlet boundary $x=L$, converges to steady states. The controlled flow rate evolution at $x=L$ is highlighted in red.

are 1 km. The simulation time is $T=12$ min. The maximum speed limit is $v_m=40$ m/s $=144$ km/h. We consider 6 lanes for the downstream freeway segment 1. Assuming the average vehicle length is 5 m plus the minimum safety distance of 50% vehicle length, the maximum density of the road is obtained as $\rho_{m,1}=6/7.5$ vehicles/m $=$ 800 vehicles/km. The upstream segment has less functional lanes thus its maximum density is $\rho_{m,2}=700$ vehicles/km. We take $\gamma_i=0.5$. The steady states $(\rho_1^\star,v_1^\star)$ and $(\rho_2^\star,v_2^\star)$ are chosen respectively as $(600$ vehicles/km$,19.4$ km/h$)$ and $(488.6$ vehicles/km$,23.8$ km/h$)$, both of which are in the congested regime and satisfy (10) and (11). The constant flow rate is $q^\star=\rho_1^\star v_1^\star=\rho_2^\star v_2^\star=11640$ vehicles/h, same for the two segments. If we consider the segment 1 with 6 lanes, then the averaged flow rate of each lane is 1940 vehicles/h/lane. The equilibrium steady state of the downstream road has higher density and lower velocity, thus is more congested than the upstream road. The relaxation time is $\tau_1=90$ s and $\tau_2=60$ s. We use sinusoid initial conditions for flow rate and velocity field which represent the stop-and-go oscillations on the connected freeway and are highlighted in the figures with blue. The two-step Lax-wendroff numerical scheme [25] is applied.

6.1 Output feedback stabilization

We consider in this traffic scenario that the downstream traffic in segment 1 is denser with slower velocity, compared with the upstream traffic in segment 2, as illustrated by the steady states. The closed-loop simulation with the collocated output feedback control input from the middle junc-

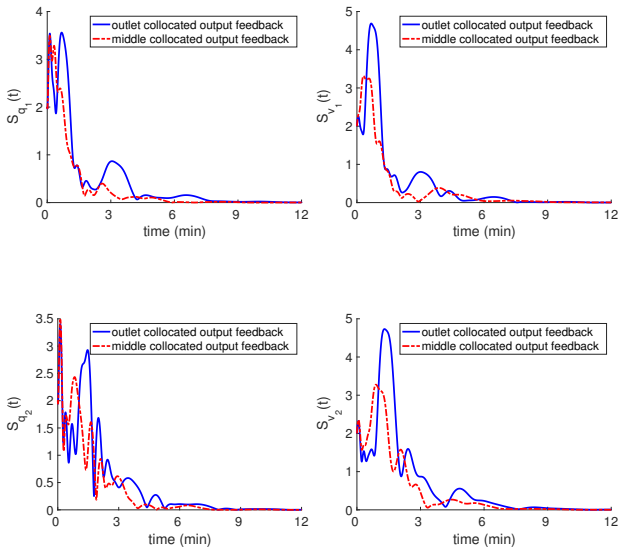

Fig. 6. Comparison of the closed-loop performance of the two collocated output feedback controllers at $x = 0$ or $x = L$.

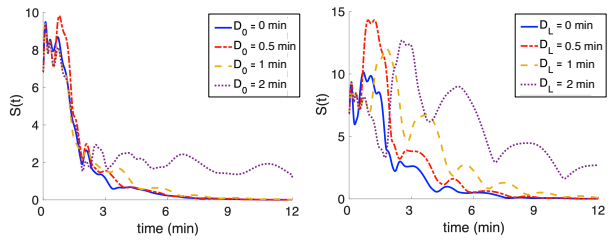

Fig. 7. The temporal evolution of $S(t)$ of the closed-loop with delayed control inputs with delay time to be 0 min, 0.5 min, 1 min and 2 min.

tion shows that the exponential convergence to the steady states is achieved simultaneously for the upstream and downstream segments in Fig. 4, where the actuated junction flow rate by the on-ramp metering is highlighted in red. Note that the steady-state velocities are different for two freeway segments and the flow rates are constant across the two segments. The output feedback stabilization with the control input and measurement of velocity and flow rate from the outlet boundary is shown in Fig. 5. The controlled flow rate at the outlet boundary is highlighted in red. Comparing the two output feedback closed-loop simulations in Fig. 4 and Fig. 5, we find out that the outlet controller takes around the same convergence time but presents a larger transient before stabilizing the system. The controlled flow rate at the middle junction with ramp metering input $U_0(t)$, highlighted in red in Fig. 4, firstly decreases such that less traffic is allowed into the downstream where traffic is denser. The controlled flow rate at the outlet with $U_L(t)$, highlighted in red in Fig. 5, increases initially such that more traffic is discharged from the segment.

To further compare the two collocated output feedback stabilization results, the closed-loop performance is demonstrated with the temporal evolution of the state variables in the spatial averaged L^2-norm, defined as

$$S_{q_i}(t) = \left| \frac{1}{L} \int_X \left(\frac{q_i(x,t) - q^\star}{q^\star} \right)^2 dx \right|^{1/2}, \tag{78}$$

$$S_{v_i}(t) = \left| \frac{1}{L} \int_X \left(\frac{v_i(x,t) - v_i^\star}{v_i^\star} \right)^2 dx \right|^{1/2}, \tag{79}$$

where $X = [-L, 0] \cup [0, L]$ represents the spatial domain of the two segments. As shown in Fig. 6, the closed-loop convergence time of both output controllers are around the same at $t = 9$ min, whereas the output feedback controller at the outlet has a larger transient for all the state variables than the output feedback at the middle junction. At around $t = 2$ min, the blue highlighted line has a bigger overshoot than the red one. In addition, the appearance of transient peaks appears later in the blue line than in the red one. We explain these observations by the different mechanisms of the proposed two controllers.

The ramp metering control input located at the downstream outlet is carried upstream by the propagation of velocity variations to mitigate traffic oscillations in both segments. In contrast, the ramp metering control input located at the middle junction works so that the actuated velocity variation at the junction travels upstream, and the actuated flow rate variations travel downstream with the traffic. Therefore, it takes a longer time for the control input to take effect on the upstream segment 2 when the output feedback is applied at the downstream outlet, whereas the output feedback at the middle junction instantly starts stabilizing both the upstream segment 2 and downstream segment 1. In addition, before the oscillations states are suppressed, the overshoot develops into a larger value and appears a bit later, as demonstrated in Fig. 6.

The proposed output feedback controllers are robust to external boundary disturbances and delays in actuation path (due to Assumption 1, [4]). Here we conduct a simulation for the closed-loop system with actuation constant delays D_0 and D_L that are respectively $0\,\text{s}, 30\,\text{s}, 60\,\text{s}, 120\,\text{s}$, where $0\,\text{s}$ represents no delay and $120\,\text{s}$ is the time length for the control input signal to traverse the two segments. Based on the definition in (78)-(79), we define an overall closed-loop performance index

$$S(t) = S_{q_i}(t) + S_{v_i}(t), \tag{80}$$

where $i = 1, 2$. Then the temporal evolution of $S(t)$ is plotted for the closed-loop system with the delayed collocated output feedback in Fig. 7.

6.2 *Comparison with PI controllers*

PI control has been applied for traffic control by ramp metering [7]. For macroscopic second-order PDE model, [39] and [40] developed PI boundary feedback controllers for the linearized ARZ model. For control of traffic on two cascaded freeway segments, boundary controllers are employed by [40] including one ramp metering at inlet $x = -L$, one ramp metering and one VSL at middle junction $x = 0$, and one VSL at outlet $x = L$, as illustrated in Fig. 8. The controlled system is fully actuated since there are four boundary

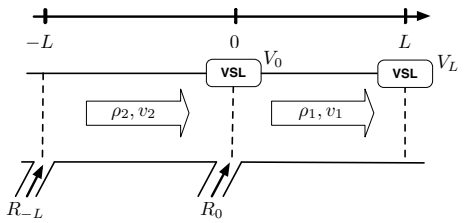

Fig. 8. The fully-actuated traffic system with two ramp metering R_{-L}, R_0 and two VSL PI controllers V_0 and V_L.

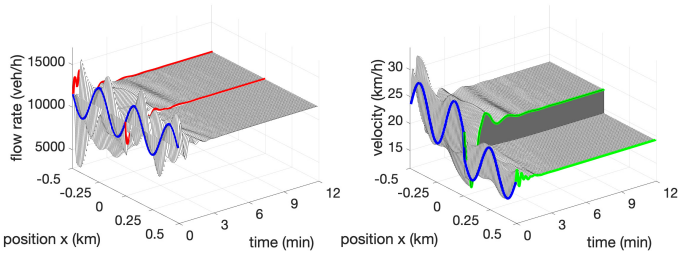

Fig. 9. The closed-loop simulation with two PI boundary feedback ramp metering controllers $R_{-L}(t)$, $R_0(t)$, highlighted in red, and two VSL PI controllers $V_0(t)$ and $V_L(t)$, highlighted with green.

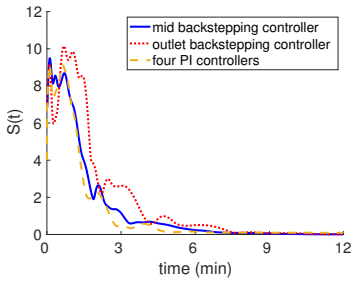

Fig. 10. The closed-loop performance with ramp metering backstepping controller $U_0(t)$, ramp metering backstepping controller $U_L(t)$ and with four PI controllers including two ramp metering $R_{-L}(t)$, $R_0(t)$, and two VSLs $V_0(t)$ and $V_L(t)$.

conditions and all of them are being actuated, whereas, in our design, only one boundary is actuated by ramp metering, either at the middle junction or at the outlet.

The four PI boundary controllers R_{-L}, R_0, V_0, V_L are defined respectively for the controlled flow rate at inlet $x = -L$, the controlled flow rate at middle junction $x = 0$, the controlled velocity at middle junction $x = 0$ and the controlled velocity at outlet $x = L$. The fully actuated boundaries are defined as

$$q_2(-L,t) = R_{-L}(t), \quad v_2(0,t) = V_0(t), \tag{81}$$

$$q_1(0,t) = R_0(t), \quad v_1(L,t) = V_L(t), \tag{82}$$

where the boundary feedback controllers are given by

$$R_{-L}(t) = q^\star + k_P^r \tilde{\rho}_2(0,t) + k_I^r \int_0^t \tilde{\rho}_2(0,t)ds, \tag{83}$$

$$V_0(t) = v_2^\star + k_P^v \tilde{v}_2(-L,t) + k_I^v \int_0^t \tilde{v}_2(-L,t)ds, \tag{84}$$

$$R_0(t) = q^\star + l_P^r \tilde{\rho}_1(L,t) + l_I^r \int_0^t \tilde{\rho}_1(L,t)ds, \tag{85}$$

$$V_L(t) = v_1^\star + l_P^v \tilde{v}_1(0,t) + l_I^v \int_0^t \tilde{v}_1(0,t)ds. \tag{86}$$

where $k_P^r, k_I^r, k_P^v, k_I^v$ are tuning gains for the upstream segment 2, $l_P^r, l_I^r, l_P^v, l_I^v$ are tuning gains for the downstream segment 1 and $q^\star, v_i^\star$ are the steady states. We use the previous model parameters and conduct the simulation under the same initial conditions such that the PI controllers can be directly compared with the control design in this paper. The tuning gains are chosen to be $k_P^r = -55, k_I^r = -0.035, k_P^v = -0.6, k_I^v = -0.025$ and $l_P^r = -10, l_I^r = -0.035, l_P^v = -0.5, l_I^v = -0.005$.

The closed-loop system behavior is shown in Fig. 9 where the temporal evolution of the four PI control inputs are highlighted, including two ramp metering in red and two VSLs in green. We then compare the closed-loop performance of the PDE backstepping controller and the PI controllers with the evolution of state variables in the spatial averaged L^2-norm, defined with $S(t)$ in (80). In Fig. 10, the closed-loop performance with the ramp metering backstepping controller at middle junction $U_0(t)$ is plotted with the blue line, the one with the ramp metering backstepping controller at outlet $U_L(t)$ is plotted in red dotted line and the one with the four PI controllers is plotted with the yellow dashed line. We can see that the convergence time and the transient is about the same for $U_0(t)$ and four PI controllers. The outlet backstepping controller $U_L(t)$ takes a relatively larger time to stabilize the system.

7 Concluding remarks

We design stabilizing output feedback control laws that guarantee the simultaneous stabilization of the traffic flow on two cascaded roads around given steady states. The flow actuation is realized with the ramp metering at the junction or the downstream outlet. The observers are designed collocated by sensing traffic velocity and flow rate at the two locations. The proposed controllers are robust to actuation delays. A more comprehensive robust control design to model parameters, external boundary, and in-domain disturbances will be of future research interest. Comparing the two collocated output feedback controllers, the middle junction one presents faster convergence and a smaller transient than the outlet one. The trade-offs between the proposed PDE backstepping controller with the PI static output feedback controllers are also discussed.

References

[1] H. Anfinsen, and O. M. Aamo, "Adaptive Control of Hyperbolic PDEs", *Springer*,2019.

[2] A. Aw, and M. Rascle, "Resurrection of "second order" models of traffic flow," *SIAM journal on applied mathematics*, vol.60, no.3, pp.916-938, 2000.

[3] J. Auriol, U.J.F. Aarsnes, P. Martin and F., Di Meglio. "Delay-robust control design for two heterodirectional linear coupled hyperbolic PDEs". *IEEE Transactions on Automatic Control*, vol.63, pp.3551-3557, 2018.

[4] J. Auriol, F. Di. Meglio, and F. Bribiesca-Argomedo, "Delay robust stabilization of an underactuated network of two

interconnected PDE systems ", *American Control Conference*, pp. 593-599, 2019.

[5] G. Bastin and J. M. Coron. "Exponential stability of networks of density-flow conservation laws under PI boundary control," *IFAC Proceedings Volumes*, vol.46(26), pp. 221-226, 2013.

[6] G. Bastin, and J. M. Coron, "Stability and boundary stabilization of 1-d hyperbolic systems ", Vol. 88. Switzerland: *Birkhäuser*, 2016.

[7] M. Papageorgiou, H. Hadj-Salem, and J.M. Blosseville, "ALINEA: A local feedback control law for on-ramp metering ", *Transportation Research Record*, 1320(1), pp.58-67, 1991.

[8] J. M. Coron, G. Bastin, and B. d'Andréa-Novel "Dissipative boundary conditions for one-dimensional nonlinear hyperbolic systems", *SIAM Journal on Control and Optimization*, vol. 45, pp.1460-1498, 2008.

[9] J. M. Coron, R.Vazquez, M. Krstic, and G.Bastin, "Local Exponential H^2 Stabilization of a $2\times$ 2 Quasilinear Hyperbolic System Using Backstepping ", *SIAM Journal on Control and Optimization*, vol.51(3), pp.2005-2035, 2013.

[10] J. M. Coron "Control and nonlinearity", *American Mathematical Society*, 2017.

[11] C. F. Daganzo, "The cell transmission model, part II: network traffic", *Transportation Research Part B: Methodological*, vol. 29(2), pp. 79-93, 1995.

[12] J. Deutscher, "Finite-time output regulation for linear 2×2 hyperbolic systems using backstepping", *Automatica*, vol. 75, pp. 54-62, 2017.

[13] J. Deutscher. "Output regulation for general linear hetero-directional hyperbolic systems with spatially-varying coefficients," *Automatica,* vol.85, pp.34-42, 2017.

[14] F. Di Meglio, R. Vazquez, and M. Krstic, "Stabilization of a system of $n+1$ coupled first-order hyperbolic linear PDEs with a single boundary input," *IEEE Transactions on Automatic Control*, vol.58(12), pp.3097-3111, 2013.

[15] F. Di Meglio, F. Bribiesca Argomedo, L. Hu, and M. Krstic "Stabilization of coupled linear heterodirectional hyperbolic PDE–ODE systems,", *Automatica,* vol 87, pp. 281-289, 2018

[16] N. Espita, H. Yu, and M. Krstic, "Event-triggered Varying Speed Limit Control of Stop-and-go Traffic," *In 21st IFAC World Congress 2020*, 2020, https://hal.archives-ouvertes.fr/hal-02931407.

[17] S. Fan, and B. Seibold, "Data-fitted first-order traffic models and their second-order generalizations: Comparison by trajectory and sensor data," *Transportation Research Record 2391,* no. 1, pp.32-43, 2013.

[18] M. Garavello, and B. Piccoli, "Traffic flow on a road network using the Aw–Rascle model", *Communications in Partial Differential Equations*, vol. 31(2), pp.243-275, 2006.

[19] G. Gomes and R. Horowitz, "Optimal freeway ramp metering using the asymmetric cell transmission model", *Transportation Research Part C: Emerging Technologies*, vol. 14(4), pp.244–262, 2006.

[20] P. Goatin and S. Göttlich and O. Kolb, "Speed limit and ramp meter control for traffic flow networks", *Engineering Optimization*, vol.48(7), pp.1121-1144, 2016.

[21] M. Gugat, M. Herty, A. Klar, and G. Leugering, "Optimal control for traffic flow networks", *Journal of optimization theory and applications*, vol. 126(3), pp.589-616, 2005.

[22] M. Herty, and M. Rascle, "Coupling conditions for a class of second-order models for traffic flow", *SIAM Journal on mathematical analysis*, vol.38(2), pp.595-616, 2006.

[23] I. Karafyllis, and M. Papageorgiou, "Feedback control of scalar conservation laws with application to density control in freeways by means of variable speed limits", *Automatica*, vol.105, pp.228-236, 2019.

[24] I. Karafyllis, and M. Krstic, "Input-to-state stability for PDEs", *Springer International Publishing*, 2019.

[25] R. J. LeVeque, " Numerical methods for conservation laws," *Basel: Birkhäuser*, vol.3, https://doi.org/10.1007/978-3-0348-5116-9, 1992.

[26] Y. Li, E. Canepa,and C. Claudel, "Optimal control of scalar conservation laws using linear/quadratic programming: Application to transportation networks", *IEEE Transactions on Control of Network Systems*, vol.1(1), pp.28-39, 2014.

[27] M. J. Lighthill, and G. B. Whitham, "On kinematic waves: II. A theory of traffic flow on long crowded roads," *Proceedings of the Royal Society of London. Series A, Mathematical and Physical Sciences (1934–1990),* vol.229 (1178), pp. 317–345, 1955.

[28] S. I. Niculescu, "Delay effects on stability: a robust control approach". *Springer Science & Business Media*, 2001.

[29] P. I. Richards, "Shock waves on the highway," *Operations Research,* vol.4 (1), pp.42–51, 1956.

[30] C. Schmuck, F. Woittennek, A. Gensior, and J. Rudolph. "Feed-forward control of an HVDC power transmission network. *IEEE Transactions on Control Systems Technology*, 22(2):597–606, 2014.

[31] M. R. Flynn, A. R. Kasimov, J. C. Nave, R. R. Rosales, and B. Seibold, "Self-sustained nonlinear waves in traffic flow," *Physical Review E*, vol.79(5), 056113, 2009.

[32] R. Vazquez, M. Krstic, and J. M. Coron, "Backstepping boundary stabilization and state estimation of a 2×2 linear hyperbolic system", *In Decision and Control and European Control Conference (CDC-ECC)*, pp. 4937-4942, 2011.

[33] H. M. Zhang, "A non-equilibrium traffic model devoid of gas-like behavior," *Transportation Research Part B: Methodological,* vol.36, no.3, pp.275-290, 2002.

[34] K. Yoshida, "Lectures on differential and integral equations", *Interscience Publishers*, Volume 10, 1960

[35] H. Yu, and M. Krstic, "Traffic congestion control for Aw-Rascle-Zhang model," *Automatica,* vol.100, pp.38-51, 2019.

[36] H. Yu, J. Auriol, and M. Krstic, "Simultaneous stabilization of traffic flow on two connected roads," *In 2020 American Control Conference (ACC),*, pp. 3443-3448. IEEE, 2020.

[37] H. Yu, J. Auriol, and M. Krstic, "Output-Feedback PDE Control of Traffic Flow on Cascaded Freeway Segments," *IFAC World Congress*, 2020.

[38] Y. Zhang and P. A. Ioannou, "Combined variable speed limit and lane change control for highway traffic", *IEEE Transactions on Intelligent Transportation Systems*, vol.18(7), pp.1812–1823, 2016.

[39] L. Zhang, C. Prieur and J. Qiao, " PI boundary control of linear hyperbolic balance laws with stabilization of ARZ traffic flow models". *Systems & Control Letters*, vol.123, pp.85-91, 2019.

[40] L. Zhang, and K. Wang, "PI Boundary Feedback Control for Freeway Traffic Networks". *In 2019 Chinese Control Conference (CCC)*, pp. 5297-5302, IEEE, 2019.